Pergamon

Cement and Concrete Research 32 (2002) 963–972

CEMENT AND CONCRETE RESEARCH

Microanalysis of alkali-activated fly ash–CH pastes

P. Jason Williams[a], Joseph J. Biernacki[a,*], Larry R. Walker[b], Harry M. Meyer[b], Claudia J. Rawn[b], Jianming Bai[b]

[a]*Department of Chemical Engineering, Tennessee Technological University, Box 5013, Cookeville, TN 38505, USA*
[b]*High Temperature Materials Laboratory, Oak Ridge National Laboratory, Oak Ridge, TN 37831, USA*

Received 8 August 2001; accepted 7 January 2002

Abstract

Samples of a Class F fly ash and calcium hydroxide (CH) hydrated in pH 13.2 sodium hydroxide solution were analyzed using backscattered electron, scanning Auger, and X-ray microanalysis. The Class F fly ash, composed mainly of aluminosilicate glass and silica, was reacted for 8, 14, and 78 days at various temperatures. These samples represent both long-term and early-age stages of hydration. Results show that a hydrate product with calcium to silica ratio near 1.4 and katoite are formed. X-ray and scanning Auger microanalysis show evidence of the formation of hydrate product on the surface of both fly ash and CH particles at early ages. This finding suggests a new mechanism to explain prior data that shows that the hydration rates increase with increasing CH–ash content in the starting mixture.

Keywords: Fly ash; $Ca(OH)_2$; Microstructure; S.E.M.; Calcium silicate hydrate (C-S-H)

1. Literature review

Fly ash is a waste material produced from combustion of coal. Due to the extensive use of coal-fired power plants and waste incinerators, by volume, fly ash is the largest produced industrial waste in the world. While fly ash is used to form blended cements, only about 20% is currently used for this purpose [1]. This application has been investigated for decades, with early papers dating back to 1960. Early researchers noted that the substitution of fly ash for cement in concrete had both economic and structural advantages [2]. Most fly ashes from the combustion of coal are made up of aluminosilicate and silica glasses plus small amounts of crystalline materials, including mullite, quartz, hematite, and magnetite [3,4]. The glasses in these ashes are sometimes pozzolanic, consuming calcium hydroxide (CH)[1] upon hydration. The partial substitution of fly ashes for cement can lead to concrete strengths equal to or greater than that for pure Portland cement after 90 days [4]. This substitution allows the formulation of high performance cement–fly ash concretes that can be produced more economically than concretes made using Portland cement alone as the binder.

The microstructure of fly ash blended cements has been thoroughly investigated by several methods including scanning electron microscopy (SEM), transmission electron microscopy (TEM), and X-ray diffraction (XRD). Most of these studies, however, investigated the microstructure of hydrated samples at ages greater than 180 days. Baalbaki et al. [5] showed that CH particles occurred around fly ash grains in a sample containing 80% cement/20% fly ash after 1 year. Rims around fly ash particles were strongly reacted and some particles were surrounded by an acicular type of calcium silicate hydrate (C-S-H). A narrow gap was observed between most fly ash particles and the surrounding paste.

An early-age study by Xu and Sarker [6] examined a 60% fly ash/40% low alkali-low tricalcium aluminate (C_3A) cement system. The results showed a fibrous cover on fly ash particles after 1 day and a shell of hydration after 7 days. At 7 days, there are CH crystals in the pores between particles and evidence that the CH may nucleate on the fly ash particles. Evidence of ettringite formation was also presented. At 28 days, CH began to redissolve and react with the fly ash. Some ash particles were found to leave a mullite sphere after

* Corresponding author. Tel.: +1-931-372-3667; fax: +1-931-372-6352.
E-mail address: jbiernacki@tntech.edu (J.J. Biernacki).

[1] Cement chemistry notation is used throughout this paper where $H = H_2O$, $C = CaO$, $S = SiO_2$, $A = Al_2O_3$, $F = Fe_2O_3$, $Mg = MgO$, $\bar{S} = SO_3$.

0008-8846/02/$ – see front matter
PII: S0008-8846(02)00734-2

reaction. At 90 days, a hydrate product formed inside fly ash spheres that had been broken during preparation.

Though there has been intense research on the microstructure of fly ash blended cements, there is less information in the literature on fly ash–CH pastes activated with alkali solutions. Shi [7,8] has published several papers dealing with the microstructure of activated lime–fly ash pastes. Shi showed that after 3 days hydration products formed on the surface of fly ash particles in lime–ash systems activated with Na_2SO_4 or $CaCl_2$. Needles and hexagonal plates on the surface of ash particles were assumed, on the basis of their morphology, to be attributed to AFm, $C_3A{\cdot}Ca(OH)_2{\cdot}12H_2O$, or C_2ASH_8. AFm phases have the general chemistry $[Ca_2(Al,Fe)(OH)_6]{\cdot}X{\cdot}xH_2O$, where X is a singly charged anion [9]. These products were also shown to form as early as 1 day in control systems that are not alkali-activated.

Fraay et al. [10] examined the dissolution of fly ash particles in a NaOH solution with a lime buffer at 7 days using TEM. At 28 days, there is evidence of surface precipitation of CH and needle-like structures on fly ash grains. Only glass particles appear to react while mullite, quartz, and iron containing particles act only as nucleation sites.

Ma et al. [11] showed the formation of hydrate products around fly ash grains in the system 90% fly ash/10% CH after 24 h at 100 °C. There was no formation of product at 25 °C for the same time period. Ma et al. [11] suggest that this difference in the hydration rate is due to the increased dissociation of the glass structure at high temperatures as shown by Pietersen [12] et al.

Fraay et al. [10] have shown that the reaction of fly ash in cement is at first controlled by the rate of CH precipitation on the surface of the fly ash and that this rate is decreased by the precipitation of C-S-H from clinker phases on the surface of the ash. The precipitation of CH is controlled by the pH of the system and increases as the extent of the hydration reaction increases which causes release of OH^- ions into the pore water. This often results in the formation of C-S-H from the hydration of fly ash in the pores, away from the surface of the ash. This suggests that the rate of reaction is a function of the rate of ash dissolution as proposed by Fraay et al. [10].

Little is known about the surface of the CH particles in an environment where there is an excess of CH. In such a system, there is no cement and oftentimes a high amount of CH that could possibly act as a site for reaction. Takemoto and Uchikawa [13] have shown that the rate of CH consumption in mixtures of CH and fly ash increases with increasing CH content of the initial mixture. They suggest that this is due to an increase in available calcium ions in the solution due to the increase in CH surface relative to ash surface. This explanation seems implausible since (1) the rates of reaction are extremely slow relative to the rate of

Table 1
Chemical composition of fly ash 9703

Component	wt.%
SiO_2	55.3
Al_2O_3	26.4
FeO	7.4
TiO_2	1.2
CaO	3.1
MgO	1.6
Na_2O	0.4
SO_3	2.9
PO_4	0.5
BaO	0.1
MnO	0.1
StO	<0.1
C	0.1
Other	0.3

Table 2
Particle size distribution of fly ash 9703 as determined using a light scattering technique

Diameter (μm)	Mass percent finer than
80.68	98
51.14	95
43.08	90
39.08	85
36.31	80
34.17	75
32.36	70
30.77	65
29.34	60
28	55
26.72	50
25.47	45
24.22	40
22.94	35
21.56	30
20	25
18.06	20
15.14	15
10.53	10
5.014	5
2.01	2

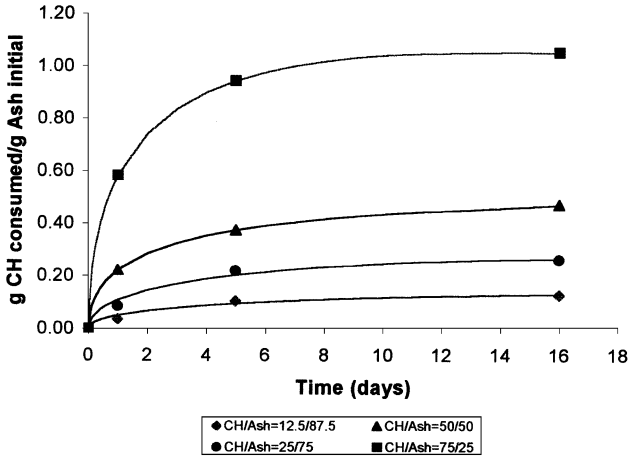

Fig. 1. TGA data showing the amount of CH consumed per initial amount of fly ash in the system reacted at 60 °C.

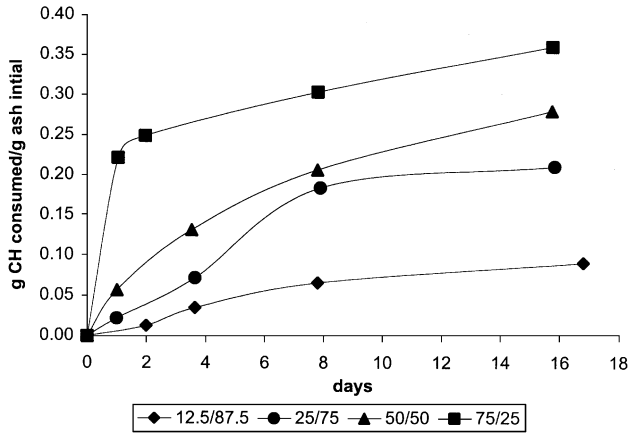

Fig. 2. Synchrotron X-ray diffraction data showing the amount of CH consumed per initial amount of fly ash in the system reacted at 40 °C.

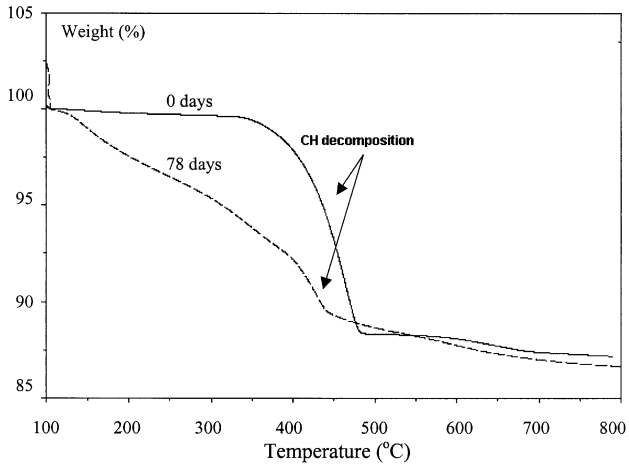

Fig. 4. TGA data showing the consumption of CH after 78 days of hydration at 60 °C in a 50:50 CH/ash mixture.

CH dissolution and transport and (2) as long as there is solid CH present the Ca^{2+} concentration in the pore solution will be set by the solubility limits of CH in the given system, not upon the amounts of available surface of CH. More recently, Biernacki et al. [14] have confirmed the experimental observations of Takemoto and Uchikawa [13]. Biernacki et al. [14] demonstrated that when the CH consumption per gram of ash is plotted as a function of time and subsequently differentiated, the CH consumption rate increases with increasing CH/ash ratio in the starting material [14]. Since ash hydration is the only reaction that consumes CH and since the C/S ratio in the product does not change appreciably, if at all, with CH/ash ratio in the starting mixture, it

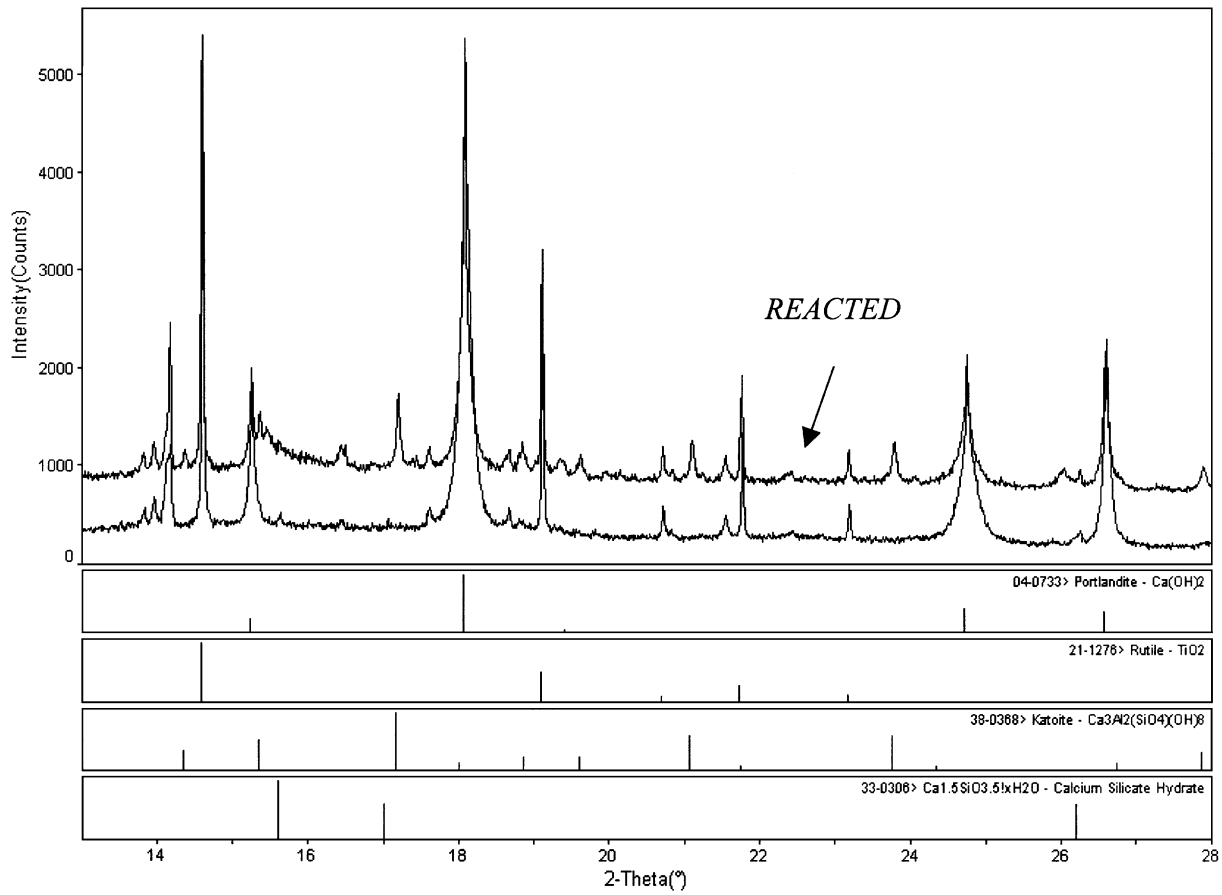

Fig. 3. Synchrotron X-ray diffraction data showing the phases present in a 50:50 CH/ash sample before and after hydration at 60 °C for 78 days.

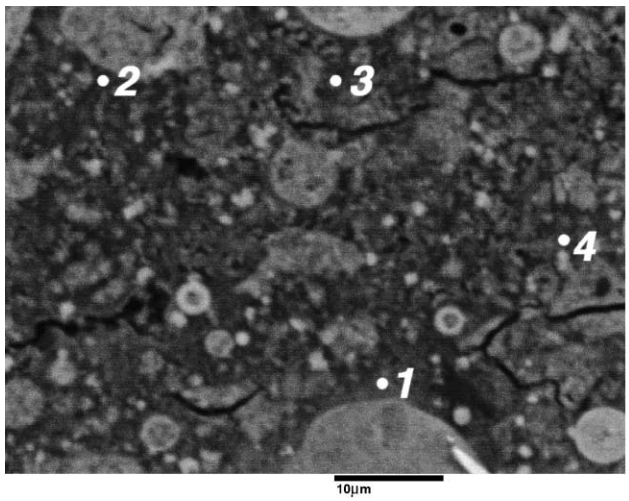

Point	CaO/SiO_2
1	1.33
2	1.47
3	1.42
4	1.48

Fig. 5. Spot analysis of a 50:50 CH/ash mixture hydrated at 60 °C for 78 days.

can be inferred that the rate of ash hydration also increases with CH/ash ratio. They also suggest a kinetic expression that assumes that the CH surface plays an active role in the reaction process, thus, making the rate proportional to both the extent of ash reaction and the extent of CH reaction. Their model, however, was not supported by experimental evidence showing that the CH surface participates actively in the reaction process. The goal of the present study is to determine whether or not all C-S-H forms on the surface of the ash or whether some can also form on the surface of the CH that is not dissolved or precipitated on ash.

2. Experimental

2.1. Materials

A fly ash from the American Coal Ash Association (ACAA) was obtained from the National Institute of Standards and Technology (NIST). This fly ash is a low-calcium type and is designated as a Class F fly ash in accordance with ASTM standard C618. The chemical composition and particle size distribution of the ash are listed in Tables 1 and 2. Reagent grade CH was obtained from Mallinckrodt.

2.2. Sample preparation

Samples of 50 wt.% CH and 50 wt.% ash were mixed by hand in a nitrogen-filled glove box to prevent carbonation of CH. When the samples appeared to be homogeneous, a 0.2-M NaOH solution was added. The water/solids ratio was kept at 0.8. This concentration of NaOH was chosen to give an initial pH above 13.2 because it has been suggested that the rate of reaction of ash is very slow below this value [10]. The samples were vigorously mixed by hand and placed in 15-ml glass vials. The vials were then placed in constant temperature baths for a predetermined amount of time. Samples were removed from the vials by breaking, yet avoiding crushing, and rapidly dried at room temperature under a vacuum. Samples were either embedded in epoxy and polished using nonaqueous polishes or broken and mounted as fracture surfaces.

2.3. SEM and X-ray microanalysis

Samples were analyzed using a JEOL 933 Electron Superprobe. Wavelength dispersive spectroscopy (WDS) was used to measure S, Mg, and Cl while energy dispersive spectroscopy (EDS) was used to measure Ca, Si, Al, Fe, K, and Ti. Not all samples were analyzed for all elements. Calibration was performed using standard reference materials including NIST SRM 466, NaCl, brotite, and FeS_2. SRM 466 is an aluminosilicate glass with composition similar to the glass phases of fly ash.

2.4. Scanning Auger analysis

Samples were also analyzed using a PHI 880 Scanning Auger Nanoprobe. Powders or fracture surfaces were mounted using doubled-sided tape. A tilted stage was used to limit electron surface charging.

2.5. Synchrotron X-ray diffraction

X-ray diffraction patterns were obtained from several samples using beamline X-14A at the National Synchrotron Light Source (NSLS). Samples were mounted in 2-mm diameter hermetically sealed borosilicate glass capillaries and revolved at 70 rpm. The patterns were recorded over a range from 8° to 28° of 2θ[2] with a step size of 0.01°/step and a counting rate of 60,000 counts/step using a Huber six-circle goniometer with a ribbed Si monochromator and

[2] Note that all 2θ values are referenced to 15-keV synchrotron radiation not to conventional Cu Kα, e.g., 8–28° 2θ at 15 keV is equivalent to 14.94–53.6° 2θ for Cu Kα radiation.

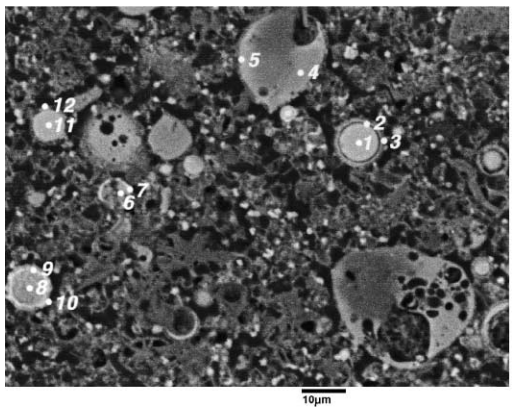

point	SiO_2	CaO	CaO/SiO_2
1	0.538	0.030	0.055
2	0.536	0.089	0.165
3	0.363	0.349	0.962
4	0.994	0.003	0.003
5	0.454	0.122	0.269
6	0.299	0.490	1.636
7	0.268	0.526	1.999
8	0.278	0.509	1.832
9	0.314	0.228	0.727
10	0.208	0.360	1.729
11	0.217	0.371	1.710
12	0.573	0.075	0.131

Fig. 6. BSE image and spot analysis of a 50:50 mixture hydrated at 60 °C for 1 day.

15-keV radiation. 10 wt.% rutile (TiO_2) was added to each sample to provide standard diffraction lines against which intensities were determined by the reference intensity ratio method. TiO_2 has peaks at $d=3.2470$, 2.4870, 2.2970, and 2.1880 Å and will not obscure or convolute peaks for CH or expected hydration products such as C-S-H ($d=3.0400$ Å) and katoite ($d=5.0460$, 4.3690, 3.3030, 2.0890, 2.7630 Å). A series of samples with different know CH/ash ratios were used as standards for estimating the amount of the different phases present.

2.6. TGA analysis

Thermalgravimetric analyses (TGA) were performed using a Thermal Advantage (TA) SDT 2960 TGA-DSC. All analyses were performed in 100 μl Al_2O_3 analysis pans in flowing argon at a rate of 10 ml/min. Samples were heated from ambient to 800 °C at a rate of 10 °C/min. Weight losses between about 350 and 600 °C were measured using a method described by Taylor [9], which uses leading and trailing derivatives as references from which to estimate step changes. This method measures losses through the midpoint of the step change.

3. Results

Systems of alkali-activated fly ash–CH mixtures were analyzed using TGA and synchrotron XRD to determine the effect of varying the fly ash/CH ratio on the rate of reaction. In these studies, several different weight ratios of constituents and temperatures ranging from 25 to 60 °C were investigated.

X-ray diffraction was used as a secondary semiquantitative technique to verify trends observed by TGA and to offer insights into hydrate product identity. Figs. 1 and 2 show the consumption of CH for a series of samples as determined by TGA and XRD analyses, respectively. Both figures show a faster rate of reaction for samples containing greater amounts of CH at very early ages implying a higher extent of ash reaction at all ages.

In these samples, the pore solutions should be saturated with CH since the solubility of CH is low, yet the results show that the consumption of CH is higher for samples with larger initial amounts of CH, e.g., the rate of CH consumption increases with increasing CH content of the starting mixture. The objective of the remaining research was to search for microstructural evidence for a reaction mechanism that could explain this behavior. Samples aged for both long and short times were studied.

To obtain long-term hydration information, samples were hydrated for 78 days at 60 °C. Figs. 3 and 4 contain XRD and TGA data, respectively, showing the depletion of the majority of CH at this age. The X-ray diffraction data shows the formation of a C-S-H phase by the characteristic broad peak at 15.614° 2θ[3] ($d=3.0400$ Å) along with considerable amounts of katoite by peaks at 9.388° 2θ ($d=5.0460$ Å, 100% peak), 10.847° 2θ ($d=4.3690$ Å), and 14.364° 2θ ($d=3.3030$ Å) at this age. Katoite is a crystalline product with the chemical formula C_3ASH_4 related to stratlingite (C_2ASH_8). As with most hydration products, this product is only partly crystalline and was, therefore, difficult to identify using XRD, though the high flux from the synchrotron X-ray source enabled lower detection limits as compared to conventional X-ray diffraction. A backscattered electron (BSE) image of this sample can be found in Fig. 5. At this stage of reaction, there is hydration product throughout the paste. There are only very small numbers of CH particles remaining, though some ash particles still retain their spherical shape. Xu and Sarker [6] suggest that the remaining ash particles are mullite or quartz spheres. XRD studies supporting this result show that mullite and quartz are generally inert to 80 days. X-ray spot analysis was used to determine the approximate concentration of the hydration product in the bulk. The C/S ratio of the hydration product is between 1.3–1.5. This is in agreement with Ma

[3] The degrees 2θ are referred to synchrotron radiation at 15 keV (λ=.82588), the C-S-H peak at ($d=3.0400$) shows up at 15.614° 2θ for 15 kV radiation where as it shows up at 29.355° 2θ for conventional Cu Kα radiation.

and Brown [15] who report a ratio of 1.4 with similar systems. Taylor et al. [16] and Rogers and Groves [17] also report the formation of C-S-H with a C/S ratio of 1.45 ± 0.2 and 1.39, respectively, in fly ash–OPC systems. It is notable to mention that these values are somewhat lower than the reported value of 1.7 for neat Portland cement pastes [9]. The C-S-H in the present system is not pure but contains traces of Fe, Al, and Mg. This is also consistent with results published by Rodgers and Groves [17] and Xu and Sarkar [6]. While the present analyses of mature pastes confirm prior reported stoichiometries, like prior studies they are unable to shed new insight on the reaction mechanism. Much earlier stages of reaction need to be investigated to discern the exact location of early age product formation.

A 50% CH/50% fly ash sample hydrated at 60 °C for 1 day was potted and analyzed using electron microscopy. Fig. 6 is an image of a selected region. The system contains high amounts of unreacted fly ash and CH. There appears to be hydrated rims around some fly ash particles. X-ray spot analysis confirms that these regions contain considerable amounts of CH but the C/S ratio does not suggest C-S-H ($C/S \sim 1.4$). Furthermore, there is no information that can be obtained about CH surfaces at this very early age. Higher extent of reaction and increased spatial resolution were required to discern hydration product.

Samples reacted for 14 days at room temperature were then analyzed. X-ray diffraction and TGA show the consumption of CH and the existence of C-S-H under these conditions, though the C-S-H is difficult to precisely determine due to superposition of the main C-S-H diffraction peaks with the CH peaks and the poor crystallinity of C-S-H [11]. Fig. 7 contains an image of a polished sample. These samples contain higher degrees of hydration than the previous sample. The BSE image appears to show the existence of hydration rims around the surface of ash particles. X-ray microanalysis, however, shows that these are not hydration rims, but rather a polishing artifact occurring due to the weak structure of very early age samples, since there is little developed microstructure available to polish and preparation of samples becomes difficult. Spot analysis confirms that the rims are silicon rich glass and not C-S-H.

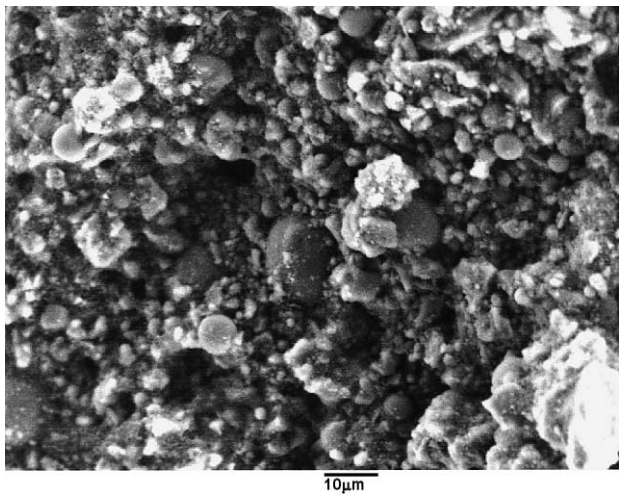

Fig. 8. Fifteen kilovolt secondary electron image of 50:50 sample hydrated for 14 days at room temperature. The image has been darkened because of surface charging.

From these images, it is impossible to determine the location of early age hydration product. Fractured samples were then used in an attempt to determine the location of hydration products in this system, though quantification of the reaction product would be difficult to obtain with fracture surfaces. Figs. 8 and 9 are a secondary electron and BSE image, respectively of fracture surfaces of a sample similar to the one above. Fig. 7 was taken using an accelerating voltage of 15 kV while Fig. 8 was taken at 10 kV. The images do not represent the same area.

The images show spherical fly ash particles surrounded by very small and irregular shaped CH particles. In both of the images, there appears to be very little evidence of reaction product on the surface of the ash particles though there are

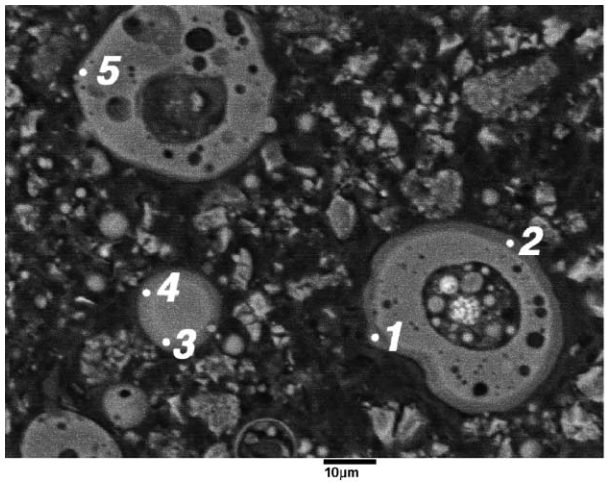

point	CaO/SiO_2
1	0.041
2	0.076
3	0.029
4	0.023

Fig. 7. Spot analysis of a 50:50 sample hydrated at room temperature for 14 days.

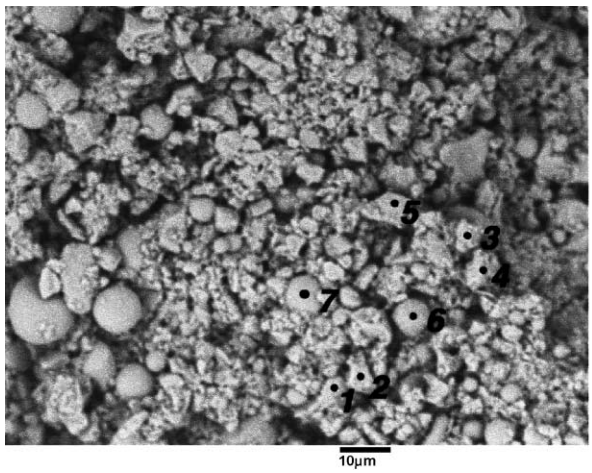

	C/S ratio		
Particle	15kV	10kV	7kV
1 *(CH)*	17.5	7.0	4.8
2 *(CH)*	26.5	9.9	6.3
3 *(CH)*	24.2	20.6	7.5
4 *(CH)*	18.5	7.2	6.7
5 *(CH)*	18.3	10.4	8.4
6 *(ash)*	0.04	0.09	0.10
7 *(ash)*	0.06	0.05	0.06

Fig. 9. Image of points chosen for spot analysis of a 50:50 CH/ash sample hydrated for 14 days at room temperature. Points 1–5 represent CH particles while 6–7 represent ash. The image is taken at 10 kV.

some areas that show precipitation of either CH or reaction product on ash surfaces. An EDS analysis was performed on regions shown in Fig. 9. In this analysis, particles were investigated using accelerating voltages of 7, 10, and 15 kV.

The results of the spot analysis are presented in Figs. 10 and 11. Increasing the accelerating voltage in the electron beam increases the depth of penetration of the electrons as explained by Heinrich [18] and Yakowitz et al. [19]. The voltage was varied in this test to determine whether or not there was a very thin surface layer of product on either ash surfaces or CH surfaces. The results show that at 15 kV the CH particles, Fig. 10, are composed of mainly calcium ($C/S > 15$) whereas the ash particles, Fig. 11, have a much higher amount of silica, as expected. As the accelerating voltage decreases, the C/S ratio increases very quickly, showing the possible existence of a silica rich layer on the surface of the CH particles, attributed to C-S-H formation. This may also be occurring on the surface of ash particles, but the decrease in the amount of silica was not as noticeable by this technique.

Monte Carlo simulations show that altering the accelerating voltage changes the depth of penetration from approximately over 2 μm at 15 kV to less than 1/2 μm at 7 kV. The results of these simulations can be found in Fig. 12. While this affords some degree of surface discrimination it is not as spatially resolved as other techniques such as scanning Auger microscopy (SAM). Since encouraging results were realized by the EDS method, Auger spectroscopy was also applied in an effort to further characterize the surface layers. When an electron beam contacts a surface, several interactions may occur. One

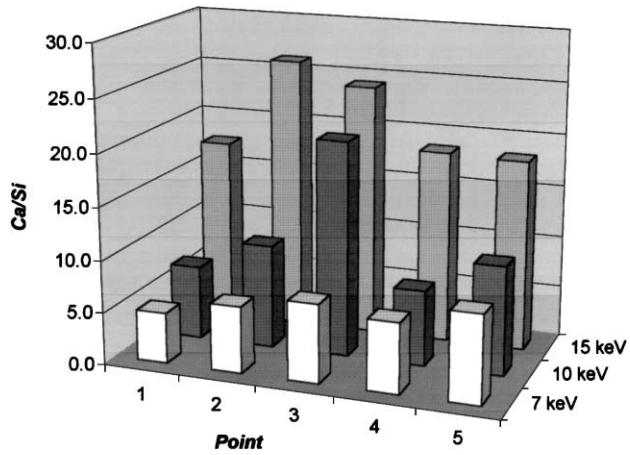

Fig. 10. Diagram of the change in Ca/Si ratio as a function of beam penetration depth on the surface of the sample. This diagram is of CH points and shows the formation of a thin, silicon-rich, layer on the surface of CH particles.

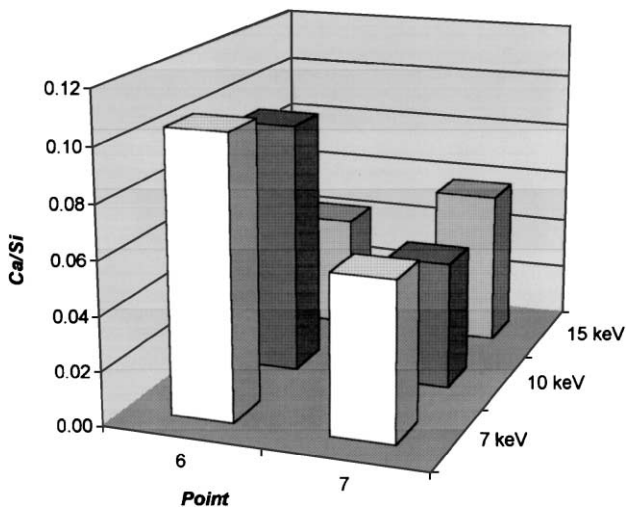

Fig. 11. Diagram of the change in Ca/Si ratio as a function of beam penetration depth on the surface of the sample. This diagram is of fly ash points and shows the formation of a thin, calcium-rich, layer on the surface of fly ash particles.

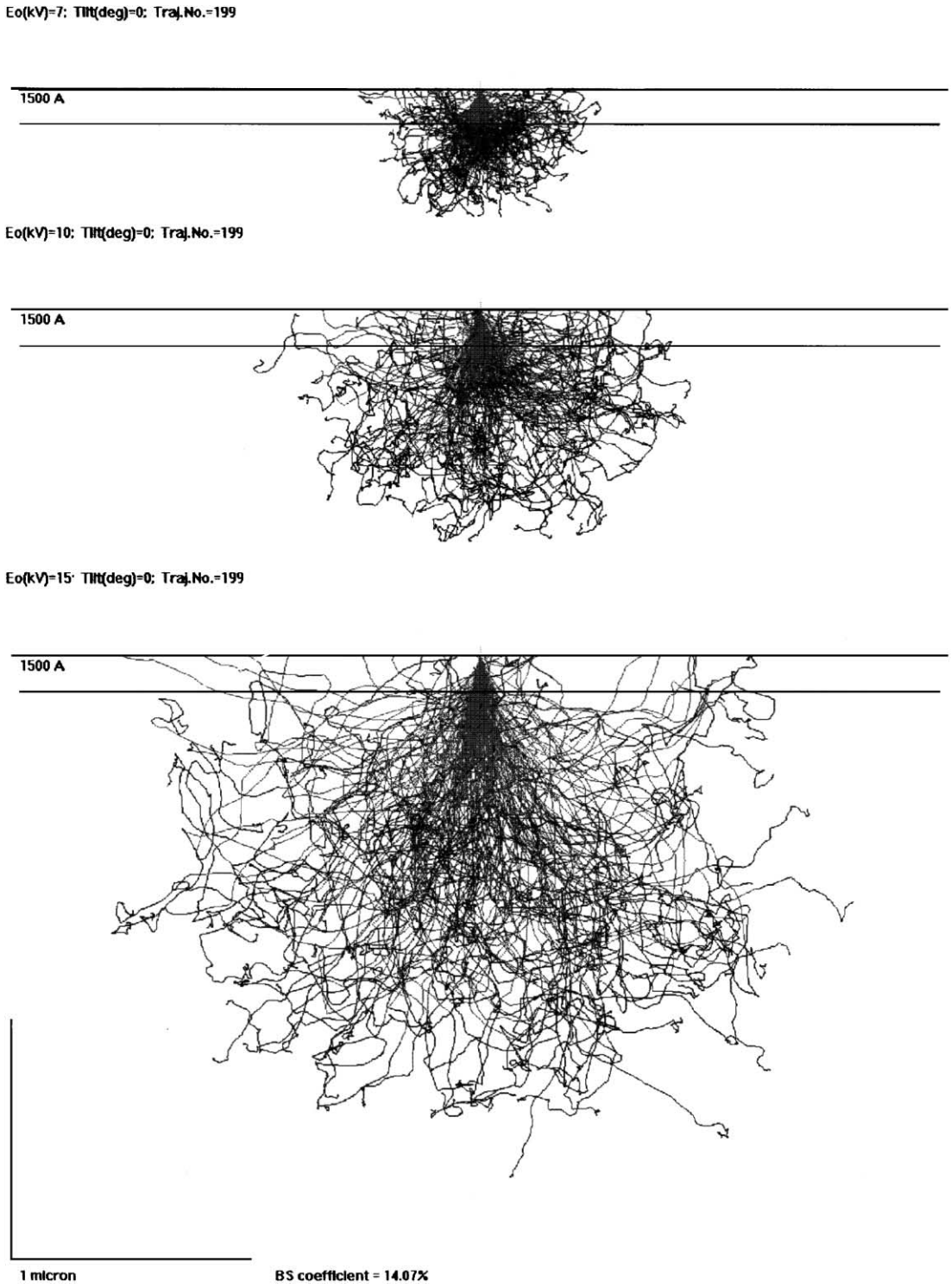

Fig. 12. Monte Carlo simulation at 7 and 15 kV on a particle of similar composition to fly ash.

such interaction is the removal of a valence electron from an inner shell. When this happens, an electron from a high energy level drops to fill the vacancy. An Auger electron is also emitted from the outer level in this process to balance the charge in the outer shell. This process can only take place on the outer one to two atomic layers of surface giving a spatial resolution on the order of 1–10 Å.

A 50%/50% wt. ash/CH mixture was hydrated for 8 days at 60 °C. This sample was chosen for reasons similar to those above. Again, powders and fracture surfaces were

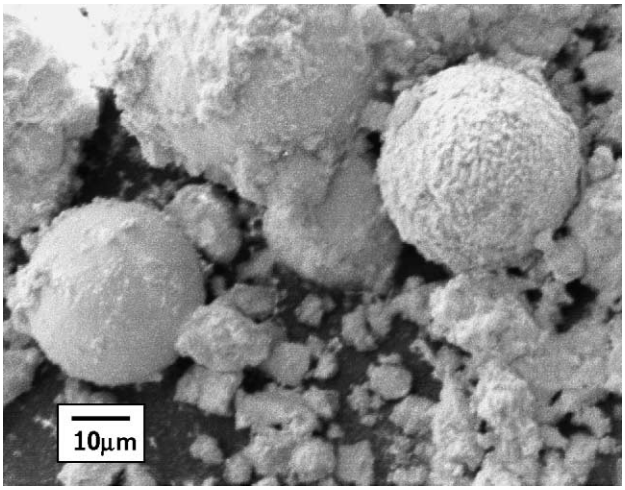

Fig. 13. Scanning electron image of a 50:50 sample hydrated for 1 day at 60 °C showing morphology of hydrate products on fly ash and CH particles.

used. SEM analysis of this sample, Fig. 13, shows morphology suggesting hydrate product on the surface of large fly ash particles. Similar morphology is found on irregular-shaped CH particles. The degree of hydration, however, for individual particles is substantially different throughout the image. Samples were analyzed by rastering the electron beam over the entire surface of a particle to obtain an average surface composition. This technique also limits beam exposure preventing problems that occur due to beam-sample interaction. If electron beams are focused on a small point for an extended period of time, interaction between the beam and the surface may dehydrate, or in other ways, alter the structure of surface materials. An image of a selected region can be found in Fig. 14.

Though several particles were analyzed, the results of three particles are presented here. The chosen particles were analyzed with the SAM and then milled using an argon ion beam. The argon ion milling beam is a variable current

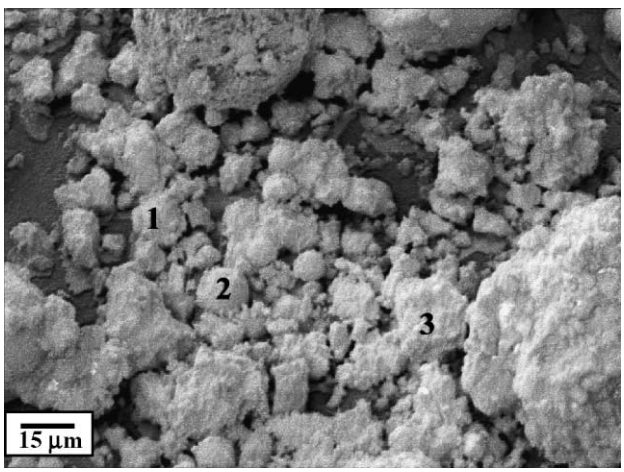

Fig. 14. Image of particles chosen for scanning Auger spot analysis.

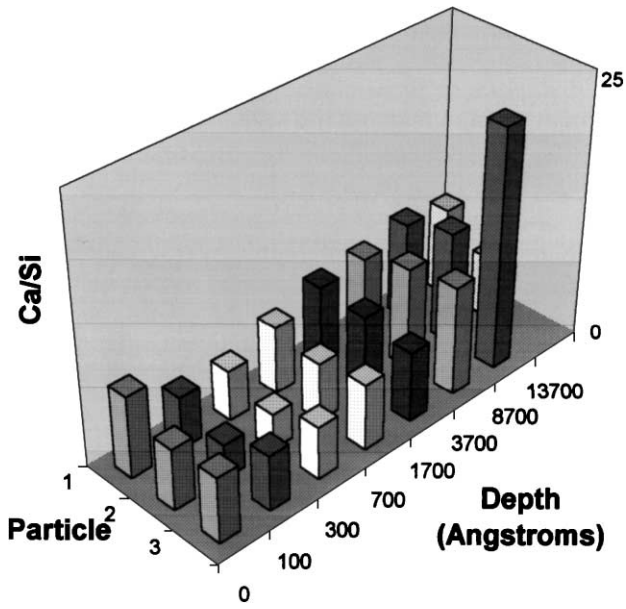

Fig. 15. Bar graph of the Ca/Si ratio as a function of beam penetration depth. Analysis was performed by milling surface away using an ion beam mill and analyzing Auger electrons.

beam that is used to remove a very small surface layer. The milling beam was used in conjunction with the Auger spectroscopy surface analysis to provide chemical information as function of depth. Figs. 15 and 16 illustrate the Ca/Si ratio as a function of depth. The C/S ratios shown on Figs. 15 and 16 are on a raw intensity basis and so are not quantitative. Particles one and two are fly ash while particle three is CH. The results confirm that a layer rich in calcium is found on the outside of all particles. At between ~100–2000 Å, a silicon rich layer similar to C-S-H is formed. This result agrees with less resolved analysis obtained from EDS that also show the formation of a C-S-H type layer on the surface of both CH and ash.

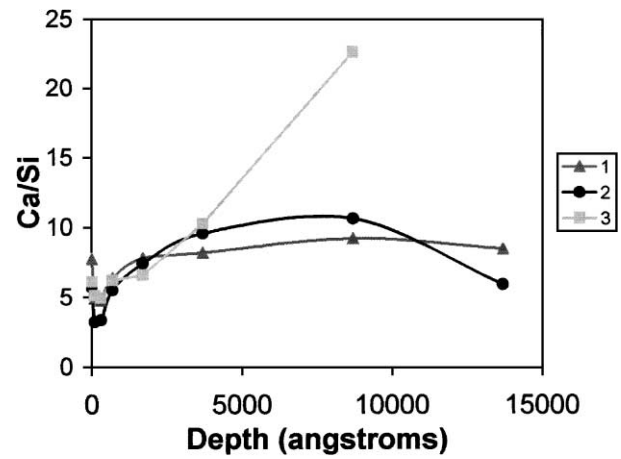

Fig. 16. Diagram of the Ca/Si ratio as a function of beam penetration depth on the surface of CH (1) and fly ash particles (2 and 3).

These surface microanalysis results suggest a reaction mechanism in which hydrate products containing both C and S precipitate on both the ash and CH surfaces. This evidence supports the observation that the rate of CH consumption increases with increasing CH content in starting CH–ash mixtures. If the rate of precipitation or surface reaction at the CH surface is similar to that observed at the ash surface, an assumption validated by these microanalysis results, then increasing the amount of available CH surface relative to ash would likely increase the observed rate of ash reaction. This evidence also offers microstructural support for the use of multiple surface kinetic models such as those proposed by Biernacki et al. [14].

4. Conclusions

This study agrees with prior results that show the formation of a C-S-H type reaction product with a Ca/Si ratio somewhat lower than that of hydrated neat Portland cement. The location of the reaction products at early ages is difficult to determine because samples had very little structure and polished surfaces were difficult to obtain. Fracture surface analysis, however, using EDS and SAM show the formation of reaction products on both the fly ash and CH surface. These results offer microstructural evidence for a reaction mechanism that involves CH as a site for the deposition and growth of hydration products, thereby explaining the observed increase in CH consumption with increasing CH content in starting mixtures.

Acknowledgments

The authors would like to thank Holnam and the Tennessee Technological University Center for the Management, Utilization, and Conservation of Water Resources for their generous ongoing support. This research was performed in part at the Oak Ridge National Laboratory on beamline X-14A at the National Synchrotron Light Source at Brookhaven National Laboratory and was sponsored by the Assistant Secretary for Energy Efficiency and Renewable Energy, Office of Transportation Technologies, as part of the High Temperature Materials Laboratory User Program, at the Oak Ridge National Laboratory, which is managed by UT-Battelle, LLC, for the US Department of Energy under contract no. DE-AC05-00OR22725.

References

[1] P.K. Mehta, Pozzolanic and cementitious by-products in concrete—another look, Proceedings of the Third International Conference Fly Ash, Slag, Silica Fume, and Natural Pozzolans in Concrete, Trondheim, Norway, vol. 1, Am. Concr. Inst., Farmington Hills, Michigan, 1989, pp. 1–43.
[2] F.P. Glasser, S. Diamond, D.M. Roy, Hydration reactions in cement pastes incorporating fly ash and other pozzolanic materials, Mater. Res. Soc. Symp. 86 (1987) 139–158.
[3] J.D. Watt, D.J. Thorne, Composition and pozzolanic properties of pulverized fuel ashes: I. Composition of fly ashes from some British power stations and properties of their component particles, J. Appl. Chem. 15 (1965) 585–594 (December).
[4] M.P. Luxan, M.I. Sanchez de Rohas, M. Frias, Investigations on the fly ash–calcium hydroxide reactions, Cem. Concr. Res. 19 (1989) 69–80.
[5] M. Baalbaki, S.L. Sarker, P.C. Aitein, H. Isabelle, Properties of microstructure of high-performance concretes containing silica fume, slag, and fly ash, Proceedings of the Fourth International Conference Fly Ash, Silica Fume, Slag, and Natural Pozzolans in Concrete, Istanbul, Turkey, Am. Concr. Inst., Farmington Hills, Michigan, 1992, pp. 921–942 (May).
[6] A. Xu, S.L. Sarkar, Microstructure development in high-volume fly–ash cement system, J. Mater. Civil Eng. 6 (1) (1994) 117–136 (February).
[7] C. Shi, Early microstructure development of activated lime–fly ash pastes, Cem. Concr. Res. 26 (9) (1996) 1351–1359.
[8] C. Shi, Pozzolanic reaction and microstructure of chemical activated lime–fly ash pastes, ACI Mater. J. 95 (5) (1998) 537–545.
[9] H.F.W. Taylor, Cement Chemistry, second ed., Thomas Telford Publishing, London, 1997.
[10] L.A. Fraay, J.M. Bijen, Y.M. de Haan, The reaction of fly ash in concrete—a critical examination, Cem. Concr. Res. 19 (1989) 235–246.
[11] W. Ma, C. Liu, P.W. Brown, S. Komarneni, Pore structure of fly ashes activated by $Ca(OH)_2$ and $CaSO_4{\cdot}H_2O$, Cem. Concr. Res. 25 (2) (1995) 417–425.
[12] H.S. Pietersen, L.A. Fraay, J.M. Bijen, Reactivity of fly ash at high pH, Mater. Res. Soc. Symp. Proc. 178 (1990) 139–157.
[13] K. Takemoto, H. Uchikawa, Hydration of pozzolanic cement, Seventh International Congress on the Chemistry of Cement, vol. 1, Editions Septima, Paris, France, 1980, pp. 2/1–2/29.
[14] J.J. Biernacki, P.J. Williams, P.E. Stutzman, Kinetics of reaction of calcium hydroxide and fly ash, ACI Mater. J. 98 (4) (2001) 380–391.
[15] W. Ma, P.W. Brown, Hydrothermal reactions of fly ash with $Ca(OH)_2$ and $CaSO_4{\cdot}2H_2O$, Cem. Concr. Res. 27 (8) (1997) 1237–1248.
[16] H.F.W. Taylor, K. Mohan, G.K. Moir, Analytical study of pure and extended portland cement pastes: II. Fly ash and cement pastes, J. Am. Ceram. Soc. 68 (12) (1985) 685–690.
[17] S.A. Rodger, G.W. Groves, Electron microscopy study of ordinary portland cement and ordinary portland cement-pulverized fuel ash blended pastes, J. Am. Ceram. Soc. 72 (6) (1989) 1037–1039.
[18] K.F.J. Heinrick, Electron Beam X-ray Microanalysis, Van Nostrand-Reinhold, New York, 1981.
[19] H. Yakowitz, D.E. Newbury, Scanning electron microscopy, in: D.E. Yohari (Ed.), Proceedings of the Ninth Annual Scanning Electron Microscopy Symposium, IITRI, Chicago, 1976, p. 151.